

On the Radiation Damage Mechanisms of Monolayer-protected Nanoparticles via TEM Analysis

Julio César Azcárate, Mariano Hernán Fonticelli, and Eugenia Zelaya

J. Phys. Chem. C, **Just Accepted Manuscript** • DOI: 10.1021/acs.jpcc.7b08525 • Publication Date (Web): 19 Oct 2017

Downloaded from <http://pubs.acs.org> on October 20, 2017

Just Accepted

“Just Accepted” manuscripts have been peer-reviewed and accepted for publication. They are posted online prior to technical editing, formatting for publication and author proofing. The American Chemical Society provides “Just Accepted” as a free service to the research community to expedite the dissemination of scientific material as soon as possible after acceptance. “Just Accepted” manuscripts appear in full in PDF format accompanied by an HTML abstract. “Just Accepted” manuscripts have been fully peer reviewed, but should not be considered the official version of record. They are accessible to all readers and citable by the Digital Object Identifier (DOI®). “Just Accepted” is an optional service offered to authors. Therefore, the “Just Accepted” Web site may not include all articles that will be published in the journal. After a manuscript is technically edited and formatted, it will be removed from the “Just Accepted” Web site and published as an ASAP article. Note that technical editing may introduce minor changes to the manuscript text and/or graphics which could affect content, and all legal disclaimers and ethical guidelines that apply to the journal pertain. ACS cannot be held responsible for errors or consequences arising from the use of information contained in these “Just Accepted” manuscripts.



On the Radiation Damage Mechanisms of Monolayer-protected Nanoparticles via TEM Analysis

Julio C. Azcárate[†], Mariano H. Fonticelli[‡], Eugenia Zelaya[†]*

[†] Centro Atómico Bariloche (CAB), CONICET, Av. Bustillo 9500, San Carlos de Bariloche,
Argentina.

[‡] Instituto de Investigaciones Fisicoquímicas Teóricas y Aplicadas (INIFTA), UNLP,
CONICET, Calle 64 y diag. 113, La Plata, Argentina.

ABSTRACT

In this work it is shown that thiol-protected Au nanoparticles (AuNPs@SR) of approximately 3.4 nm in size suffered unexpectedly high radiation damage under standard transmission electron microscopy (TEM) operating conditions. For metallic systems (conducting sample) it is expected that the greatest contribution to the damage to come from knock-on displacement, but radiolysis is the most probable radiation damage mechanism for organic samples. The radiation damage of the electron beam produce huge changes in AuNPs' structure, leading to coalescence of the Au cores when their {100} surface are facing each other. The complete coalescence process involve thiol desorption, AuNPs' reorientation and surface diffusion of Au adatoms, which produce the oriented attachment of the Au cores. The knock-on displacement cannot explain by itself the time taken by the entire process. Through a rigorous analysis we rationalize the results

1
2
3 considering that because of the small size of AuNPs they have a lower electron density than the
4
5 bulk material, which favors radiolytic damage.
6
7

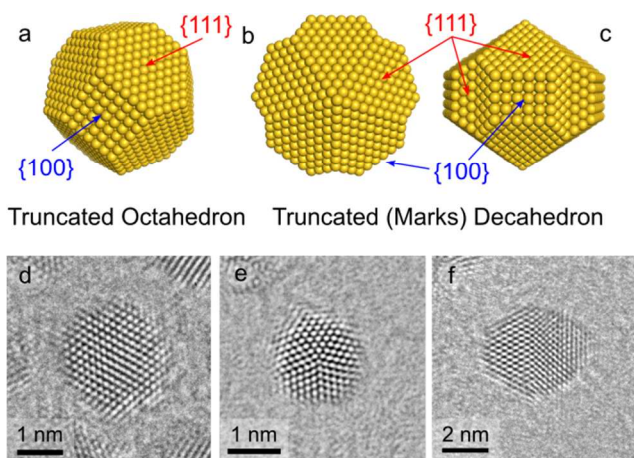
8 9 **Introduction**

10
11 Most of the advanced analytical techniques involve some kind of radiation (photons or
12
13 electrons are the most popular) to analyze the sample. It is well known that the interaction
14
15 between radiation and matter can cause sample damage, which must be thoughtfully
16
17 characterized and taken into account for correct data interpretation.
18
19

20
21 Transmission electron microscopy (TEM) is an advanced technique where electrons are
22
23 accelerated up to energies of hundreds of keV across the sample to obtain structural information.
24
25 In materials science, TEM has huge importance and the radiation damage it produces has been
26
27 extensively studied for bulk materials. Nevertheless, the radiation damage in new materials like
28
29 those based on nanoparticles is less explored.
30
31

32
33 Nanoparticles (NPs) acquired great interest in the last few years and many novel applications
34
35 are based on them. Thiol capped gold NPs (AuNPs@SR) are one of the most studied NPs and
36
37 they are considered a model systems when compared with those constituted of other metals.
38
39 AuNPs@SR can be synthesized by several methods depending of the nature of the thiols. The
40
41 two-phase approach by Brust and Schiffrin¹ is extensively used because it allows excellent size
42
43 control by tuning the thiol/metal ratio. It leads to narrow size distributions for NPs < 6 nm.²
44
45 However, some fundamental features like chemical composition and structure are not completely
46
47 described or known. Moreover, the analysis of composition, size and structure performed by
48
49 different and complementary techniques do not always lead to compatible results.^{3,4} In those
50
51 cases it is of paramount importance the understanding and quantification of radiation-damage
52
53 processes.^{5,6}
54
55
56
57
58
59
60

1
2
3 The AuNPs@SR present the fcc structure of Au, however they change their shape according to
4 their size. Different geometries for AuNPs were widely reported in literature.⁷⁻¹¹ Figure 1 shows
5 the most commonly observed shapes in the present work: a truncated octahedron (a) and a
6 truncated decahedron (Marks Decahedron) (b and c). These geometries are described for bare
7 (uncapped) or weak-ligand capped NPs. The truncated octahedron (Figure 1a and 1d) is the most
8 stable geometry according to thermodynamic arguments,⁹ and their faces are crystalline planes of
9 the $\{111\}$ and $\{100\}$ families of an fcc structure. The case of the truncated decahedron described
10 by Marks corresponds to pentagonally twinned NP, with plane faces exposing the above
11 mentioned families of planes ($\{111\}$ and $\{100\}$). Nevertheless, it is well known that thiols alter
12 the surface structure of NPs due to their strong covalent bonds with metallic atoms.^{6,12} Figures
13 1d-f show HRTEM images of AuNPs@SR with shapes similar to the above models near the
14 $[011]$ axis zone (Figures 1a-c). Here, a projection of the $\{111\}$ and the $\{100\}$ surfaces along the
15 $[011]$ axis zone can be observed.



33
34
35
36
37
38
39
40
41
42
43
44
45
46
47
48
49
50
51
52
53
54
55
56
57
58
59
60
Figure 1: Sphere-models representation of (a) a Truncated Octahedron and (b-c) of a Truncated (Marks) Decahedron. (d-f) Representative examples of AuNPs@SR imaged in HRTEM mode.

It is well known that electron radiation causes damage on samples during a TEM session.¹³ The radiation damage may have different origins depending on the nature of the samples and the

1
2
3 operation parameters. The radiation damage was widely studied for bulk materials like metals
4 (conducting), semiconductors, and inorganic solids or polymers (insulators). Electron radiation
5 damage acts by several mechanisms depending on the scattering type: *Elastic* or *Inelastic*. Elastic
6 scattering occurs by electrostatic deflection of the electron beam due to the Coulomb field of the
7 atomic nuclei. This scattering gives electron-diffraction patterns and phase contrast in TEM
8 images. In both cases, the elastic scattering leads to the so-called knock-on displacement,
9 producing changes in the atomic positions or sputtering of the surface atoms. On the other side,
10 inelastic scattering occurs by the Coulomb interaction between the electron beam and the atomic
11 electrons of the sample. This scattering induces electronic excitation which produces secondary-
12 electrons, emission of X-rays, and can also be responsible for radiolysis effects or heating.¹⁴
13
14 There are several papers on radiation damage of particles since the 80's decade to these days, but
15 most of them were performed on bare NPs¹⁵⁻¹⁸ instead of capped NPs^{19,20}. However, the
16 radiation damage mechanism was not explored in detail. For this reason, it is paramount to
17 deeply study the consequences of electron irradiation damage on capped-NPs.
18
19

20
21
22 The aim of this paper is the characterization and analysis of the main sources of radiation
23 damage over AuNPs@SR during TEM imaging. The changes that NPs suffered were recorded in
24 HRTEM images over time. First, we described the observed AuNPs coalescence induced by
25 electron beam irradiation during HRTEM imaging. Thus, a careful HRTEM analysis under
26 different operation condition (varying exposure doses) have shown that two AuNPs coalesce
27 only when the {100} planes face each other (oriented attachment). This interesting result was
28 confirmed for representative pairs of nanoparticles' geometries (two truncated octahedrons,
29 truncated octahedron and Marks' decahedron, and two Marks' decahedrons). Then, the different
30 causes of damage –knock-on, radiolysis and thermal heating– were considered and the effect
31
32
33
34
35
36
37
38
39
40
41
42
43
44
45
46
47
48
49
50
51
52
53
54
55
56
57
58
59
60

1
2
3 they can have on AuNPs@SR was estimated. We concluded that the main cause of radiation
4 damage is attributed to radiolysis process, which cannot be avoided in HRTEM mode at room
5 temperature. In this operation mode the radiation damage can drastically alter the sample,
6
7 leading to AuNPs@SR coalescence.
8
9
10
11

12 **Experimental**

13
14
15 Synthesis of AuNPs@SR: the nanoparticles were prepared using the two liquid phases method
16 developed by Brust and Schiffrin.¹ First, 137 mg of tetraoctylammonium bromide, TOABr
17 (Sigma-Aldrich) were dissolved in 8 mL of toluene (Carlo Erba) in a round bottom flask. Then, 4
18 mL of HAuCl₄ 25 mM solution (0.1mmol of Au) in HCl 100 mM were added and the mixture
19 was stirred until the complete transfer of AuCl₄⁻ to the toluene phase. The aqueous phase was
20 removed and the toluene solution was washed once with 5 ml of H₂O to remove the acid excess.
21
22 Afterwards, under constant stir, 9 μL of dodecanethiol (Sigma-Aldrich) were added to the
23 mixture. After 10 minutes, 38 mg of NaBH₄ in 3 mL of H₂O were added quickly. The stir was
24 kept for 3 hs to promote a narrow size distribution. Both phases were separated, and toluene was
25 evaporated keeping a tenth of this liquid phase. AuNPs were purified by precipitation with 15
26 mL of ethanol, and were centrifuged after 30 min. This purification procedure was repeated three
27 times.²¹ Then, the AuNPs were dried and stored as powder at -18°C.
28
29
30
31
32
33
34
35
36
37
38
39
40
41
42

43 Specimen preparation: the AuNPs were redispersed in toluene and then drop-casted on 300
44 mesh ultrathin carbon film on holey carbon support copper grids.
45
46
47

48 TEM imaging and data analysis: Two transmission electron microscopes were used to carry
49 out the radiation damage studies: a Phillips CM200 UltraTwin (LaB₆) and a FEI Tecnai F20 G2
50 (FEG), both operated at 200 keV. The current measurements were developed using a Gatan 646
51 Double Tilt Analytical Holder connected to a Keithley 6485 Picoammeter.
52
53
54
55
56
57
58
59
60

1
2
3 HRTEM images simulation were carried out with JEMS software.²² The proper orientation of
4
5 atomic models of NPs for simulation were made using a software developed in the physics of
6
7 metals division at Centro Atómico Bariloche.²³
8
9

10 **Results and Discussion**

11
12 At the start of the TEM observation, the bright field images of the sample revealed the
13
14 presence of NPs spread across the entire carbon film. However, after some minutes of
15
16 observation of the same area, a coalescence of particles can be obtained. The figure 2 shows the
17
18 difference between the fresh sample and the particles observed by HRTEM after a few minutes.
19
20 The particles viewed at first time were round and homogeneously dispersed, as can be seen
21
22 outside the green coloured area. The particles observed in HRTEM mode or bright field
23
24 condition presented the same characteristics at the green colored area. However, they look rather
25
26 bigger than at the beginning and not as rounded as the particles viewed for the first time. The
27
28 size distribution was obtained from images taken at the same magnification of not irradiated
29
30 areas; it was fitted with a lognormal function resulting in a mean diameter of $3.4 \text{ nm} \pm 0.8 \text{ nm}$
31
32 (see Supplementary Information).
33
34
35
36
37
38

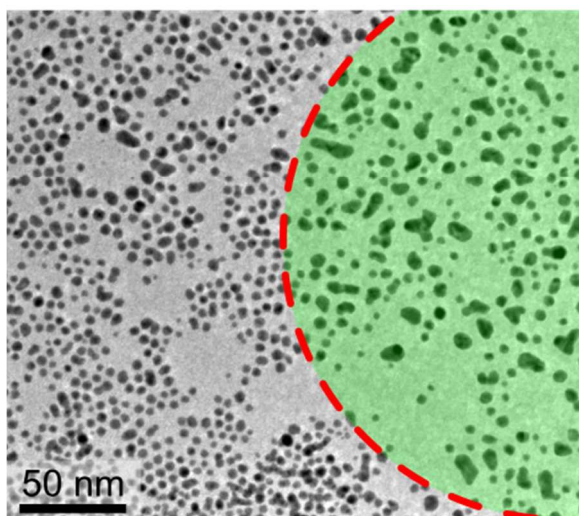


Figure 2: Bright field image of AuNPs@SC12. The green marked zone was previously observed in HRTEM condition. The image is slightly underfocus to reinforce the contrast.

Next, it will be shown that the electron beam induces coalescence and ripening processes. Because most of the nanoparticles were found to be truncated octahedrons and truncated (Marks) decahedrons, in what follows we present studies of radiation damage for both kind of nanoparticle shapes. The first pair of particles were two truncated octahedrons (Figure 3). The nanoparticles are expected to be randomly oriented before their irradiation. However, most of the particles are preferentially oriented along a low-index zone axis.

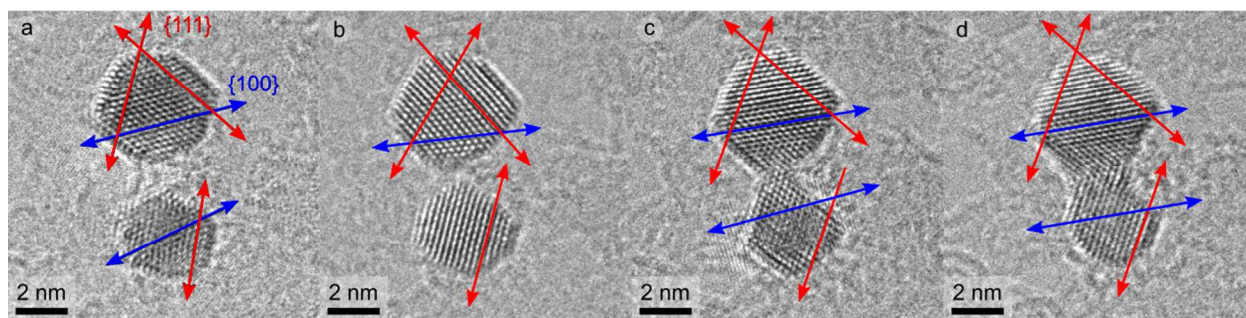


Figure 3: Coalescence of two truncated octahedron like AuNPs. Red arrows represent the planes type $\{111\}$ and the blue ones $\{100\}$ along the $[011]$ zone axis. The images were taken at: a) 1037 s, b) 1097 s, c) 1158 s and d) 1195 s after start irradiation.

Figure 3 shows the coalescence of two truncated octahedrons when $\{100\}$ planes of each particle are facing to each other. In the beginning -Figure 3a and Figure 3b-, the planes $\{111\}$ and $\{100\}$ from one particle are not aligned with the same family of planes of the other. In Figure 3c the $\{100\}$ faces of each octahedron are close to be parallel. At this point, the shape of the octahedron at the bottom of this panel starts to change. It seems that few Au atoms form a column between the two AuNPs. Moreover, there is no evidence of boundaries between the particles. This HRTEM image was simulated to corroborate that both AuNPs are at the same height with both planes $\{100\}$ facing each other (see Supplementary Information). Finally, in

1
2
3 Figure 3d it could be distinguished a unique orientation for the {111} and the {100} families of
4 planes. Furthermore, the evolution of the two octahedron system continued until the formation of
5 a unique faceted NP was reached. This coalescence process where two particles joint to form a
6 new bigger one is also called *Smoluchowski ripening*.²⁴ An increase in the roughness of the
7 amorphous carbon substrate is also evident which a consequence of electron beam radiation
8 damage is.
9

10
11 It is worth to mention at this point that the coalescence seems to be reached after the
12 reorientation of the {111} and {100} planes of the NPs, which is attributed to an “electron
13 wind”.²⁵ This reorientation is evident in the smaller nanoparticles. Even more, the nanoparticles'
14 displacements can be as large as their sizes. However, this pivot is not observed in the bigger
15 NPs due to their higher masses (moment of inertia).
16
17

18
19 At this point, the coalescence observed looks similar to the previously reported on bare
20 AuNPs,^{17,18} but in this case the AuNPs are capped by an alkanethiolate monolayer. The first
21 question is: RS monolayer is still on AuNPs? In order to describe the coalescence of two
22 particles of similar sizes, two scenarios are considered. In the simplest reasoning, the
23 particles coalesce when their naked surfaces encounter. Previously, the radiation damage
24 must have stripped-off the RS moieties at least from the {100} faces. In a more complex
25 reasoning, if the capping-agent were still on the {100} faces that stick each other the
26 adsorbates should leave both faces within about a minute while coalescing (Figures 3c-d,
27 4d-e and 5b-g). In other words, a concerted movement of the RS species should occur, in
28 order to lead to a single fcc structure like the ones observed in the figures 3d, 4e and 5g.
29 Furthermore, this concerted mechanism could also be done across {111} faces and not only
30 across {100} faces. But coalescence was not observed across {111} (see below). On the
31
32
33
34
35
36
37
38
39
40
41
42
43
44
45
46
47
48
49
50
51
52
53
54
55
56
57
58
59
60

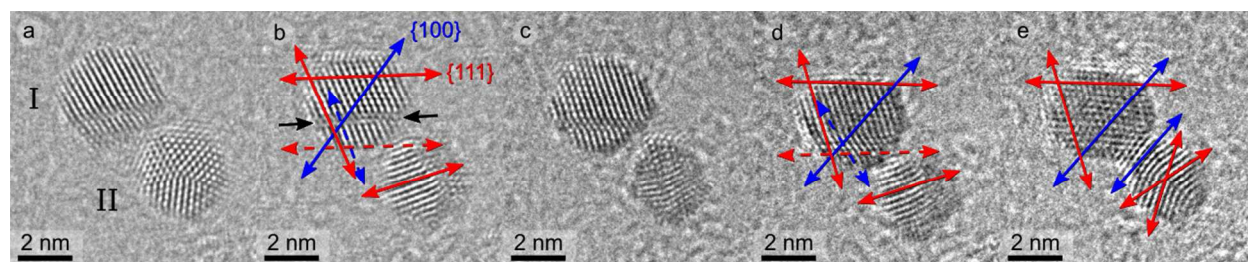
1
2
3 other hand, as the total metallic core surface decrease due to the coalescence, the RS
4 moieties could not simply rearrange over the new formed particle because their coverage
5 would increase. However, when the size increases the coverage decreases^{2,26} to the same
6 value as the self-assembled monolayer on flat surfaces.²⁶ In a simple calculation, two
7 nanoparticles of similar sizes than those shown in Figure 3 are formed by 976 Au atoms
8 and 187 RS chains (3 nm) and 314 Au atoms and 91 RS chains (2nm), respectively.² The
9 coalescence of these AuNP@RS would lead a bigger one of 1290 Au atoms and 221 RS
10 chains (3.2 nm)². However, the sum of RS chains of both individual AuNP@RS are higher
11 than the expected (57 RS chains in excess). Also for this reason, the second mechanism
12 does not seem to be probable.

13
14
15 It is clear that at least the {100} faces must be free of adsorbed molecules (uncapped or bare).
16
17 Otherwise, the coalescence process shown in Figure 3 would not occur. Notably, it was reported
18 that the coalescence processes of two naked NPs is a spontaneous and non-activated processes.¹⁹

19
20
21 The electron radiation damage could produce the total or partial desorption of the adsorbed
22 thiols. However, it is not clear up to now whether the adsorbates leave the surface as thiolate,
23 thiyl, radical fragments and/or some of the reported staples.^{3,27} After thiol desorption, the
24 exposed metallic surface of a NP can get in contact with the bare surface of a surrounding NP,
25 thus producing their coalescence.

26
27
28 It is commonly believed that the increase in temperature is responsible for the adsorbate
29 desorption. However, the electron beam heating is overestimated,⁷ and the calculation of the
30 temperature rise shows an increase of less than 2 K in AuNPs smaller than 10 nm (See
31 Supplementary Information for details in calculation).

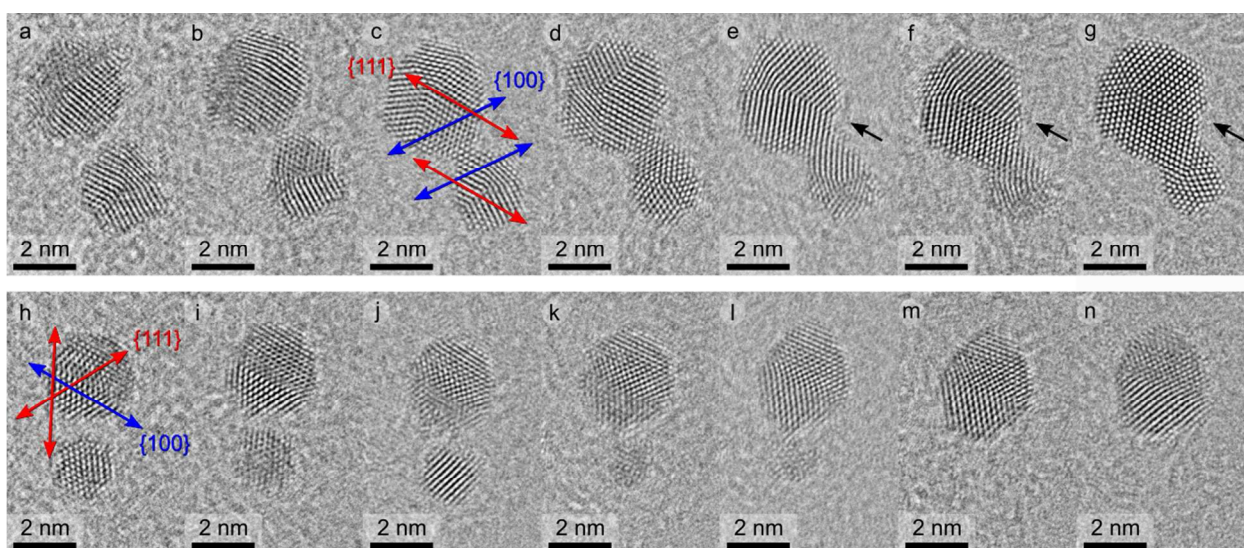
1
2
3 As a second case study, Figure 4 shows the coalescence of a twinned truncated (I) octahedron
4 and a truncated decahedron (II) AuNPs. Once again, the coalescence process starts just when the
5 {100} faces of both NPs are facing each other (Figure 4e). The black arrows (Figure 4b) are
6 showing the stacking fault planes where the {111} and {100} planes are in similar directions. It
7 is interesting to note that the atomic planes rearrange, so that the stacking fault vanishes. Only
8 when it seems to disappear, the coalescence between both AuNPs starts. It is noticeable that just
9 before coalescence, Figure 4d, the truncated octahedral NP (I) does not expose a complete {100}
10 surface to the other NP. This observation suggests that coalescence occurs when equal planes are
11 facing each other. Even more, this result suggests that if the existence of a defect avoids the
12 facing of the {100} faces, the coalescence would not occur until the defect disappears.



27
28
29
30
31
32
33
34
35
36 Figure 4: Coalescence of a twinned truncated octahedron (I) and a truncated decahedron (II). The
37 images were taken at: a) 346 s, b) 390 s, c) 463 s, d) 498 s and e) 553 s after start irradiation. The
38 red arrows indicate the planes {111} and the blue ones {100} planes along the [011] zone axis.
39 Black arrows show the stacking fault plane, and the dashed arrows show planes in the other side
40 of this plane.
41
42
43
44
45
46
47
48

49 The last processes to be illustrated involve two pairs of truncated (Marks) decahedrons (Figure
50 5). These AuNPs were all together in the same region and received exactly the same radiation
51 dose. The two particles in the top-panels (Figure 5 a-g) show, once again, the coalescence
52 through the {100} faces of both AuNPs. In the other case (Figure 5 h-n), the bottom AuNP
53
54
55
56
57
58
59
60

1
2
3 reduces its size over time until it disappears. This mechanism was reported and described as an
4
5 Ostwald ripening process, which was previously observed by STEM.¹⁹ On the contrary, the
6
7 particles bigger than ~2nm seem to coalesce when the {100} faces encounter. The Ostwald
8
9 ripening occur by unbalanced atomic diffusion from the smaller NPs to the bigger one. On the
10
11 basis of computer simulations it was proposed that Ostwald ripening can be induced by
12
13 electronic irradiation occur without thiol desorption.¹⁹ However, the system could be trapped on
14
15 local energy minimum, which could impede the full Ostwald ripening process. Also, the Ostwald
16
17 ripening on a totally naked AuNP is not favored.¹⁹ Nevertheless, the presented results suggest
18
19 that the ripening is favored when the {100} faces are naked. In all cases, after coalescence,
20
21 the new formed particle suffer a rearrangement of their atoms to get a shape with a lower surface
22
23 energy. This is evident in the Figure 5e-g, where the arrows indicate the vertex changes on the
24
25 bigger (up-left) particle. This kind of rearrangement of the surface atoms was reported for
26
27 different metallic NPs.^{28,29}
28
29
30
31
32
33



52
53 Figure 5: Four truncated (Marks) decahedron suffering coalescence (a-g) and ripening (h-n).
54
55 These AuNPs were nearby and consequently exposed to the same radiation doses. The AuNPs
56
57
58
59
60

1
2
3 are near to the [011] zone axis. The images were taken at: (a;h)=110 s, (b;i)=170 s, (c;j)=274 s,
4
5 (d;k)=361 s, (e;l)=385 s, (f;m)=460 s and (g;n)= 485 s.
6
7

8
9 Noticeably, no coalescence nor ripening events were observed between surfaces that exposed
10 planes different from the {100}, even when two nearby NPs rotate (or pivot) during a long time
11 (see Supplementary Information, Figure SI 3). In these cases, it is observed that nanoparticles'
12 crystalline planes are not aligned. Moreover, both coalescence processes do not depend on the
13 received doses, but on nanoparticles' orientation: the most important factor in coalescence
14 phenomena here described is the parallel alignment of the {100} faces.
15
16

17
18 All these results suggest that at least the {100} faces are uncovered by thiols when the
19 coalescence occurred. This can be explained considering that radiation damage can induce thiol
20 desorption. Indeed, migration of Au atoms and Au-SR moieties were reported for the case of
21 ripening.¹⁹ In this direction it is proper to analyze the possible mechanisms of radiation damage
22 involved in the capping degradation.
23
24

25 26 27 28 29 30 31 32 33 34 35 **Analysis of Mechanism Involved in Radiation Damage**

36
37 After discarding the temperature increase as a significant source of sample damage, two main
38 mechanisms involved in this kind of radiation damage still remains: Knock-On displacement (by
39 elastic scattering) and Radiolysis (by inelastic scattering). Knock-On displacement involves the
40 energy transfer during elastic scattering between the incoming electron and the atomic nucleus of
41 the sample. The energy transferred could displace the atom away from their natural vibrational
42 position, giving the breakdown of several chemical bonds. The term "radiolysis" involves several
43 chemical changes induced by inelastic interaction between the incoming electrons with the
44 atomic electrons in the sample. The inelastic scattering produce electronic excitation or
45 ionization which could relax by several ways (e.g. chemical bonds scission). The chemical bonds
46
47
48
49
50
51
52
53
54
55
56
57
58
59
60

1
2
3 scission implies atomic displacements. The necessary conditions for this atomic displacements
4
5 are localization of an electronic excitation with sufficient energy and for sufficiently long times
6
7 (longer than the time for an atomic vibration, or ~ 1 ps). That mechanical relaxation of the
8
9 surrounding atomic cores leads to a bonding instability, in many cases involving displacement of
10
11 atomic cores. In this way the potential energy inherent in electronic excitations can be converted
12
13 to momentum of a departing atom nucleus.³⁰ For conducting materials, like metals, the electrons
14
15 in their conductive bands compensate extremely fast (~ 1 fs) the ionization processes or collective
16
17 electronic excitation (plasmonic excitation) decreasing the radiolysis effects.³⁰ However, in non-
18
19 conductive materials, like organic materials, the charge reposition is not so fast to avoid chemical
20
21 scission due to electronic rearrangements of excitation or ionization. The nanoparticles studied
22
23 here should not be considered a priori nor as a typical conducting materials nor as an insulator.
24
25 Then, it is necessary to evaluate and compare both mechanisms to determine which one is the
26
27 most important. This could help to establish possible strategies to avoid or diminish the TEM
28
29 radiation damage. Egerton reported in several articles and reviews about TEM and SEM
30
31 radiation damage.^{14,31,32} Cross-section values (σ) or critical doses (De) were determined for
32
33 different bulk materials. In the next paragraphs, both mechanisms are described and compared.

40
41 First, we analyzed the atomic displacement produced by elastic scattering, which can occur in
42
43 all kind of samples but is evident in crystalline specimens (blurring the electron diffraction
44
45 pattern). In order to estimate the cross sections for knock-on events, σ_d , we will start focusing on
46
47 a few relevant magnitudes: the energy of the incident electrons, E_0 , the maximum energy
48
49 transferred by knock-on impact of an incoming electron, E_{max} , and the energy needed to get an
50
51 atomic displacement, E_d . When $E_{max} < E_d$, displacement damage is absent since the incident
52
53 energy is bellow certain threshold incident energy (E_0^{th}). E_0^{th} is above 200 keV for most of the
54
55
56
57
58
59
60

1
2
3 elemental solids, but its value is considerably lower for organic materials (lighter elements).

4
5 According to Egerton *et al.* E_{max} , is given by³¹:

$$E_{max} = \frac{E_0(E_0 + 2m_0c^2)}{\left[E_0 + \left(1 + \frac{m_0}{M} \right)^2 \frac{Mc^2}{2} \right]} \approx \frac{2E_0(E_0 + 2m_0c^2)}{Mc^2}$$

6
7
8
9
10
11
12 where m_0 is the electron rest mass, c is the speed of light and M is the mass of the knocked
13
14 atom. Note that the energy transferred rises as the energy of the incident electrons increases, and
15
16 it is larger for lighter elements. On the other hand, the displacement energy, E_d , strongly depends
17
18 on the strength and number of bonds in which the specific atom participate. In the case of small
19
20 NPs most of the atoms are on the surface. For this reason, it is proper to consider that sputtering
21
22 displacement is more important than “bulk” knock-on damage. Thus, the AuNPs@SC12’ surface
23
24 chemistry might be considered in some detail in order to get reliable results. Another drawback
25
26 comes from the fact that displacement energies E_d are not well known for organic molecules.
27
28 Nevertheless, an estimation of the total atom bond energy can be used instead E_d as good
29
30 approximation.³² Two models of thiol adsorption has been reported: on bridge “standard” site
31
32 and staple motif. Recently, it was proposed that thiols adsorb as thiyli moieties rather than
33
34 thiolate moieties.³³ Henceforth, the RS moieties represent either kind of chemical species, thiyli
35
36 or thiolate. In the standard model, the sulfur atom is bonded on bridge sites of a perfect Au(hkl)
37
38 surfaces.^{33–35} In the staple motif model two RS moieties are bonded to an Au adatom, and also to
39
40 the Au surface atoms (Au-RS-Au_{ad}-RS-Au).^{33–35} For the Au(111) surface the energy per RS unit
41
42 is lower in the staple configuration than for the bridge site. Notably, the opposite was reported
43
44 for Au(100), being the adsorption on the bridge site more favorable than on a staple motif.³⁵ In
45
46 our calculation we have chosen the adsorption energy that corresponds to the less stable RS
47
48 moiety (i.e RS in a bridge site of an Au(111) surface; adsorption energy of -1.5 eV)³³, which is
49
50
51
52
53
54
55
56
57
58
59
60

equivalent to the greater knock-on cross-section (see below). The energy for Au on Au(111) surface is -3.44 eV and for Au on borders is -3.12 eV.³⁴ The bond dissociation energy of the relevant covalent bonds are: C-H 4.2 eV; C-C 3.7 eV and C-S 3.2 eV (as an approximation, it is considered that these energies are the same than those on an alkanethiol molecule).³⁶ As an example for AuNPs@SC12 consider that a sulfur atom is displaced when two bonds are broken: one between sulfur and the alkyl carbon (S-C) and the other between sulfur and gold (Au-S), taking into account the different models on RS adsorption. The energy E_d is the sum of every broken bond. The atom displaced is bold labelled in Table 1 and Figure 6. Table 1 shows the E_d values considered in each displacement case. These estimated values for E_d can be used to calculate the cross section for knock-on, σ_d , displacement as:³²

$$\sigma_d = (0.25\text{barn})F(v)Z^2 \left[\frac{E_{max}}{E_d} - 1 \right]$$

where $F(v) = \gamma^{-2}(v/c)^{-4} = (1 - v^2/c^2)(v/c)^{-4}$, and Z is the atomic number of the displaced atom. Clearly, the probability to get an atomic displacement increases with the atomic number, but decreases with the atomic mass. Then, the mean time between damage events (τ) could be estimated from:

$$\tau = \frac{1}{J\sigma_d}$$

where J is the electron flux. Figure 6 shows the variation of the atomic displacement cross section as a function of the energy of the incident beam. The most probable displacement by knock-on at 200 keV acceleration voltage corresponds to the sulfur atom (Au-S-chain). Note that for this electron-acceleration it is infrequent to displace gold atoms off the metallic surface (Au-Au_s-S). Thus, the reduction of the acceleration voltage, a standard strategy to reduce the knock-on damage, would have negligible effect in the Au atoms displacement. In addition, the

1
2
3 displacement of total thiol molecule was considered (**Au-S-chain**), but its cross-section is
4
5 smaller than that of amorphous carbon. All in all, the time required for each damage event is
6
7 very long. While on average it takes ~ 17 min to displace a sulfur atom by knock-on (Table 1),
8
9 the time required to observe coalescence, which necessarily implies many damage events, was
10
11 shorter than this figure (10^2 s). Moreover, as a direct comparison between theoretical and
12
13 experimental data could not be straightforward, we also considered a lower E_d (higher cross
14
15 section) for Au-S-C knock-on displacement. If one half of the previously used E_d was taken (i.e
16
17 $E_d = 2.4$ eV for Au-S-C) the time per each damage event will be ~ 8 minutes. Then, the S
18
19 displacement by knock-on should not be considered as the main source of radiation damage. In
20
21 the same way, the knock-on displacement cannot explain the migration of Au atoms or Au-SR
22
23 moieties between NPs necessary for the *Ostwald Ripening* process.¹⁹ In figure 6 the knock-on
24
25 cross section curves for Au atoms on borders and Au-SR moieties (orange and green dashed
26
27 lines, respectively) show that they would only be displaced if the energy of the incoming
28
29 electrons is bigger than 200 keV.
30
31
32
33
34
35
36

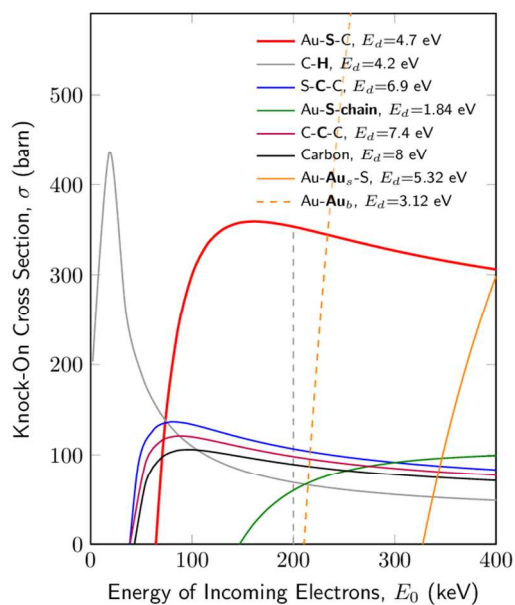


Figure 6: Knock-On cross section for atomic displacements of different atoms and molecular moieties on alkanethiol protected gold nanoparticles.

Table 1: Bond types and cross sections for knock-on and radiolysis as mechanisms of radiation damage. Accelerating voltage = 200 keV, $J = 2.8 \times 10^{18} \text{ e} \cdot \text{s}^{-1} \cdot \text{cm}^{-2}$.

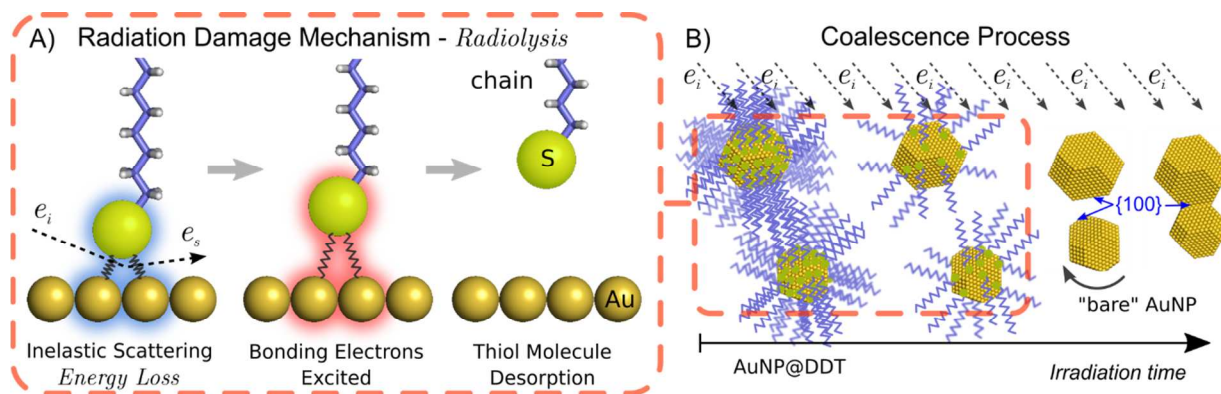
Bond	E_d (eV)	σ_d (barn)	τ (s)	Mechanism
Nanoparticles³⁴				
Au-Au _s -S	5.32	-	-	Knock-On
Au-S-C	4.7 (~2.4) ^a	355 789	1006 453	Knock-On
Au-S-chain	1.84	59	6053	Knock-On
S-C-C	7	105	3401	Knock-On
C-C-C	7.4	98	3644	Knock-On
C-H	4.2	60	5952	Knock-On
Bulk Mat.³¹				
Carbon film	8	89	4013	Knock-On
Organic		10^5 - 10^8	4-0.004	Radiolysis
Inorganic		0.1 - 10^6	40000-0.4	Radiolysis
Conducting	10-50	10^2 - 10^3	4000-400	Sputtering

^a sub-estimation of the E_d value considering the half of the calculated value for both bonds scission.

The last radiation damage mechanism to be studied is radiolysis, which is associated with inelastic scattering. The energy loss of the incoming electrons can produce electronic transitions in the sample. One of the effects of these electronic transitions is to drive chemical reactions between organic or inorganic species. Radiolysis is, in general, less important in conducting materials like metals. For the sake of comparison, Table 1 presents the displacement energy, E_d ,

1
2
3 cross section and the involved mechanism in alkanethiol capped gold nanoparticles. The range of
4 values for radiolysis cross sections reported in the literature for organic or inorganic bulk
5 samples is also shown.
6
7
8
9

10 Thiol capped nanoparticles could not be classified as typical organic, inorganic or metallic
11 materials. They are not conducting materials -as bulk metals are- and could be similar to either
12 organic molecules or inorganic materials. Furthermore, the smaller NPs have discrete electronic
13 levels similar to molecules.²⁷ Whatever the chemical nature chosen for the comparison was, the
14 time-scale of the radiolysis events is by far smaller than those estimated for knock-on
15 displacements. Moreover, considering that radiolysis causes electronic excitation in the sample,
16 it is expected that the frontier molecular orbitals close to the sulfur atom were affected. Then, it
17 is reasonable to hypothesize that RS units and/or Au_s-S-chain units would detach from the NPs'
18 surface before the coalescence or ripening processes starts. Scheme 1, panel A, represents the RS
19 desorption due to radiolysis. The thiol desorption is a necessary but not sufficient condition for
20 the coalescence of the nanoparticles. According to our experimental findings the particles
21 coalesce only when two RS free {100} faces encounter (Scheme 1, panel B). This can be
22 explained considering that the electron flux produce their pivot and/or rotation.
23
24
25
26
27
28
29
30
31
32
33
34
35
36
37
38
39
40
41
42
43
44
45
46
47
48
49
50
51
52
53
54
55
56
57
58
59
60



Scheme 1: (A) Radiolysis as the main radiation damage mechanism before the AuNPs coalescence. (B) RS desorption, followed by coalescence of AuNP@DDT under the electron beam in TEM. Compare with HRTEM images of Figure 3.

Further reasoning is needed to understand why only the {100} faces are involved in coalescence and ripening. On one side, the thiol (and/or Au_s-S-chain units) would be detached through radiolysis processes irrespective of the surface orientation ({100} or {111} faces). The thermodynamic driving force for crystal growth is the decrease in total energy. This decrease is the reason of the Ostwald ripening. For the oriented attachment observed in this study the same principle is applicable, neglecting entropy changes.³⁷ The surface energy of solids is related to their sublimation enthalpy. For FCC crystals, the surface energy ratio between faces {111} and {100} is $\gamma_{\{111\}}/\gamma_{\{100\}} \cong 0.87$ (see Supplementary Information). This means that {100} faces are more energetic than {111} faces, hence the coalescence across {100} faces is thermodynamically favored. On the other side, several early studies on Pt and Au NPs showed the atomic reconstruction of the {100} face.^{7,16,28} This atomic reconstruction is a clear example about the higher surface energy of {100} faces.

Conclusion

1
2
3 This study explains the mechanism by which AuNP@SR are affected by the electron beam in
4 the TEM. The radiation damage produces considerable sample modification when Au
5 nanoparticles protected by alkanethiols are imaged in high-resolution TEM under standard
6 operation conditions. The lack of understanding of the physical process involved during TEM
7 characterization can lead to a wrong characterization of this kind of nanosystems. We observed
8 that the particles can approach each other, and suffer coalescence and ripening as a consequence
9 of their irradiation. Interestingly, these processes only occur between nearby particles when the
10 {100} surfaces face each other, but they were not observed among other crystal orientations.
11 Furthermore, the radiation damage does not depend on received doses but it does depend on
12 crystal orientation.
13
14
15
16
17
18
19
20
21
22
23
24
25
26

27 The coalescence of thiol protected AuNPs only occur if their protecting monolayer is stripped
28 of, which implies the thiol molecules desorption. The desorption of the thiol of {100} surfaces
29 face seems to be the most probable scenario in order to maintain the stability of the coalesced
30 particle. Otherwise, the number of total RS chains available of the two original particles would
31 overcome the maximum calculated for the coalesced particles. This thiol desorption is probably
32 the main effect of radiation damage during a characterization routine by TEM. The actual time
33 needed to coalesce NPs is shorter than the time of damage calculated taking into account only
34 knock-on radiation damage. For this reason, the main radiation process that favors the
35 coalescence is radiolysis rather than knock-on. The radiolysis induces the RS desorption, at least,
36 from the Au(100) surfaces. Otherwise, no coalescence would be observed. Furthermore, being
37 the radiolysis the main source of radiation damage, partial or complete RS desorption is a
38 probable scenario. In this context, the coalescence of the resulting naked AuNPs is more
39 probable through the {100} faces due to their relative surface energy. The deep analysis of all of
40
41
42
43
44
45
46
47
48
49
50
51
52
53
54
55
56
57
58
59
60

1
2
3 the probable irradiation damage mechanisms affecting a nanosystem gives another frame to the
4
5 TEM characterization of this kind of materials. The nature of the radiation damage shows that
6
7
8 the AuNPs behave more like as an insulating material than a conductor when irradiated in the
9
10
11 TEM, which is interpreted as a size-effect.

12
13 The proper study of radiation damage of each sample is needed to arrive to confident
14
15 interpretation of materials behavior.
16
17

18 19 20 ASSOCIATED CONTENT

21
22
23 **Supporting Information.** AuNPs size distribution, HRTEM images simulations, calculation
24
25 about temperature increase, A listing of the contents of each file supplied as Supporting
26
27

28 29 AUTHOR INFORMATION

30 31 32 **Corresponding Author**

33
34 * E-mail: jcazcarate@cab.cnea.gov.ar (J.C.A.). Tel: +54-294-4445548. Fax: +54-294-4445299.

35
36
37 Web: <https://fisica.cab.cnea.gov.ar/metales>
38
39

40 41 42 **Author Contributions**

43
44 The manuscript was written through contributions of all authors. All authors have given approval
45
46 to the final version of the manuscript.
47

48 49 50 **Funding Sources**

51
52 The Consejo Nacional de Investigaciones Científicas y Técnicas (CONICET) PIP 0333,
53
54 Universidad Naniocional de La Plata (UNLP), Comisión Nacional de Energía Atómica (CNEA)
55
56 and Universidad Nacional de cuyo (UNCuyo) support this work.
57
58
59
60

1
2
3 **Notes**
4

5
6 The authors declare no competing financial interest.
7

8
9 **ACKNOWLEDGMENT**
10

11
12 The authors express their thanks to Adriano Geraci for the technical support and Dr. M.T.
13 Malachevsky for his assistance in the manuscript edition.
14
15
16

17
18 **REFERENCES**
19

- 20
21 (1) Brust, M.; Walker, M.; Bethell, D.; Schiffrin, D. J.; Whyman, R. Synthesis of Thiol-
22 Derivatised Gold Nanoparticles in a Two-Phase Liquid–Liquid System. *J. Chem. Soc.,*
23 *Chem. Commun.* **1994**, No. 7, 801–802.
24
25
26
27
28 (2) Hostetler, M. J.; Wingate, J. E.; Zhong, C.-J.; Harris, J. E.; Vachet, R. W.; Clark, M. R.;
29 Londono, J. D.; Green, S. J.; Stokes, J. J.; Wignall, G. D.; et al. Alkanethiolate Gold
30 Cluster Molecules with Core Diameters from 1.5 to 5.2 Nm: Core and Monolayer
31 Properties as a Function of Core Size. *Langmuir* **1998**, *14*, 17–30.
32
33
34
35
36
37
38 (3) Azcárate, J. C.; Corthey, G.; Pensa, E.; Vericat, C.; Fonticelli, M. H.; Salvarezza, R. C.;
39 Carro, P. Understanding the Surface Chemistry of Thiolate-Protected Metallic
40 Nanoparticles. *J. Phys. Chem. Lett.* **2013**, *4*, 3127–3138.
41
42
43
44
45
46 (4) Corthey, G.; Giovanetti, L. J.; Ramallo-López, J. M.; Zelaya, E.; Rubert, A. A.; Benitez,
47 G. A.; Requejo, F. G.; Fonticelli, M. H.; Salvarezza, R. C. Synthesis and Characterization
48 of Gold@Gold(I)–Thiomalate Core@Shell Nanoparticles. *ACS Nano* **2010**, *4*, 3413–3421.
49
50
51
52
53
54 (5) Azcárate, J. C.; Floridia Addato, M. A.; Rubert, A.; Corthey, G.; Kürten Moreno, G. S.;
55 Benítez, G.; Zelaya, E.; Salvarezza, R. C.; Fonticelli, M. H. Surface Chemistry of
56
57
58
59
60

- 1
2
3 Thiomalic Acid Adsorption on Planar Gold and Gold Nanoparticles. *Langmuir* **2014**, *30*,
4 1820–1826.
5
6
7
8
9 (6) Corthey, G.; Olmos-Asar, J. A.; Casillas, G.; Mariscal, M. M. M.; Mejía-Rosales, S.;
10 Azcárate, J. C.; Larios, E.; José-Yacamán, M.; Salvarezza, R. C.; Fonticelli, M. H.
11 Influence of Capping on the Atomistic Arrangement in Palladium Nanoparticles at Room
12 Temperature. *J. Phys. Chem. C* **2014**, *118*, 24641–24647.
13
14
15
16
17
18
19 (7) Marks, L. D. Experimental Studies of Small Particle Structures. *Reports Prog. Phys.* **1999**,
20 *57*, 603.
21
22
23
24
25 (8) Buffat, P. A. A. Electron Diffraction and HRTEM Studies of Multiply-Twinned Structures
26 and Dynamical Events in Metal Nanoparticles: Facts and Artefacts. *Mater. Chem. Phys.*
27 **2003**, *81*, 368–375.
28
29
30
31
32
33 (9) Barnard, S. S.; Lin, X. M.; Curtiss, L. A. Equilibrium Morphology of Face-Centered
34 Cubic Gold Nanoparticles >3 Nm and the Shape Changes Induced by Temperature. *J.*
35 *Phys. Chem. B* **2005**, *109*, 24465–24472.
36
37
38
39
40
41 (10) Wang, Z. W.; Palmer, R. E. Determination of the Ground-State Atomic Structures of Size-
42 Selected Au Nanoclusters by Electron-Beam-Induced Transformation. *Phys. Rev. Lett.*
43 **2012**, *108*, 245502.
44
45
46
47
48
49 (11) Marks, L. D.; Peng, L. Nanoparticle Shape, Thermodynamics and Kinetics. *J. Phys.*
50 *Condens. Matter* **2016**, *28*, 53001.
51
52
53
54 (12) Olmos-Asar, J. A.; Ludueña, M.; Mariscal, M. M. Monolayer Protected Gold
55 Nanoparticles: The Effect of the Headgroup–Au Interaction. *Phys. Chem. Chem. Phys.*
56
57
58
59
60

- 1
2
3
4
5
6
7
8
9
10
11
12
13
14
15
16
17
18
19
20
21
22
23
24
25
26
27
28
29
30
31
32
33
34
35
36
37
38
39
40
41
42
43
44
45
46
47
48
49
50
51
52
53
54
55
56
57
58
59
60
- 2014, *16*, 15979.
- (13) Stenn, K.; Bahr, G. F. Specimen Damage Caused by the Beam of the Transmission Electron Microscope, a Correlative Reconsideration. *J. Ultrastruct. Res.* **1970**, *31*, 526–550.
- (14) Egerton, R. F.; Li, P.; Malac, M. Radiation Damage in the TEM and SEM. *Micron* **2004**, *35*, 399–409.
- (15) Bovin, J.-O.; Wallenberg, R.; Smith, D. J. Imaging of Atomic Clouds Outside the Surfaces of Gold Crystals by Electron Microscopy. *Nature* **1985**, *317*, 47–49.
- (16) Wallenberg, L. R.; Bovin, J.-O.; Petford-Long, A. K.; Smith, D. J. Atomic-Resolution Study of Structural Rearrangements in Small Platinum Crystals. *Ultramicroscopy* **1986**, *20*, 71–75.
- (17) Flüeli, M.; Buffat, P. A.; Borel, J.-P. Real Time Observation by High Resolution Electron Microscopy (HREM) of the Coalescence of Small Gold Particles in the Electron Beam. *Surf. Sci.* **1988**, *202*, 343–353.
- (18) Surrey, A.; Pohl, D.; Schultz, L.; Rellinghaus, B. Quantitative Measurement of the Surface Self-Diffusion on Au Nanoparticles by Aberration-Corrected Transmission Electron Microscopy. *Nano Lett.* **2012**, *12*, 6071–6077.
- (19) Gutiérrez-Wing, C.; Olmos-Asar, J. A.; Esparza, R.; Mariscal, M. M.; Yacamán, M. J. The Role of Ad-Atoms in the Coalescence of Alkanethiol-Passivated Gold Nanoparticles. *Electrochim. Acta* **2013**, *101*, 301–307.
- (20) Yuk, J. M.; Jeong, M.; Kim, S. Y.; Seo, H. K.; Kim, J.; Lee, J. Y. In Situ Atomic Imaging

- 1
2
3 of Coalescence of Au Nanoparticles on Graphene: Rotation and Grain Boundary
4 Migration. *Chem. Commun.* **2013**, *49*, 11479.
5
6
7
8
9 (21) Azcárate, J. C. Estudio Sobre La Modificación de Nanopartículas Metálicas Para El
10 Desarrollo de Sensores Fluorescentes Fotomodulables, Universidad Nacional de La Plata,
11 2014.
12
13
14
15
16
17 (22) Stadelmann, P. The Java Electron Microscopy Software (JEMS). *Lausanne Interdiscip.*
18 *Cent. Electron Microsc.* **2012**.
19
20
21
22 (23) Barragan, E. CParticulas. *CParticulas (GitHub)* **2016**,
23 <https://doi.org/10.5281/zenodo.572995>. (accessed Oct 9, 2017)
24
25
26
27
28 (24) Smoluchowski, M. V. Drei Vortrage Uber Diffusion, Brownsche Bewegung Und
29 Koagulation von Kolloidteilchen. *Zeitschrift fur Phys.* **1916**, *17*, 557–585.
30
31
32
33 (25) Marks, L. D.; Zhang, J. P. Is There an Electron Wind? *Ultramicroscopy* **1992**, *41*, 419–
34 422.
35
36
37
38
39 (26) Olmos-Asar, J. a; Rapallo, A.; Mariscal, M. M. Development of a Semiempirical Potential
40 for Simulations of Thiol-Gold Interfaces. Application to Thiol-Protected Gold
41 Nanoparticles. *Phys. Chem. Chem. Phys.* **2011**, *13*, 6500–6506.
42
43
44
45
46
47 (27) Walter, M.; Akola, J.; Lopez-Acevedo, O.; Jadzinsky, P. D.; Calero, G.; Ackerson, C. J.;
48 Whetten, R. L.; Grönbeck, H.; Häkkinen, H. A Unified View of Ligand-Protected Gold
49 Clusters as Superatom Complexes. *Proc. Natl. Acad. Sci.* **2008**, *105*, 9157.
50
51
52
53
54
55 (28) Wallenberg, L. R.; Smith, D. J.; Petford-Long, A. K.; Wallenberg, L. R.; Bovin, J. O.
56 Dynamic Atomic-Level Rearrangements in Small Gold Particles. *Science* **1986**, *233*, 872–
57
58
59
60

- 1
2
3 875.
4
5
6
7 (29) Casillas, G.; Velázquez-Salazar, J. J.; Jose-Yacaman, M. A New Mechanism of
8 Stabilization of Large Decahedral Nanoparticles. *J. Phys. Chem. C* **2012**, *116*, 8844–8848.
9
10
11 (30) Hobbs, L. W. Radiation Effects in Analysis of Inorganic Specimens by TEM. In
12 *Introduction to Analytical Electron Microscopy*; Hren, J. J., Goldstein, J. I., Joy, D. C.,
13 Eds.; Springer US: Boston, MA, 1979; pp 437–480.
14
15
16 (31) Egerton, R. F.; McLeod, R.; Wang, F.; Malac, M. Basic Questions Related to Electron-
17 Induced Sputtering in the TEM. *Ultramicroscopy* **2010**, *110*, 991–997.
18
19
20 (32) Egerton, R. F. Mechanisms of Radiation Damage in Beam-Sensitive Specimens, for TEM
21 Accelerating Voltages Between 10 and 300 kV. *Microsc. Res. Tech.* **2012**, *75*, 1550–1556.
22
23
24 (33) Reimers, J. R.; Ford, M. J.; Halder, A.; Ulstrup, J.; Hush, N. S. Gold Surfaces and
25 Nanoparticles Are Protected by Au(0)–thiyl Species and Are Destroyed When Au(I)–
26 thiolates Form. *Proc. Natl. Acad. Sci.* **2016**, *113*, E1424–E1433.
27
28
29 (34) Mariscal, M. M.; Olmos-Asar, J. A.; Gutierrez-Wing, C.; Mayoral, A.; Yacaman, M. J. On
30 the Atomic Structure of Thiol-Protected Gold Nanoparticles: A Combined Experimental
31 and Theoretical Study. *Phys. Chem. Chem. Phys.* **2010**, *12*, 11785–11790.
32
33
34 (35) Hu, G.; Jin, R.; Jiang, D. Beyond the Staple Motif: A New Order at the Thiolate–gold
35 Interface. *Nanoscale* **2016**, *8*, 20103–20110.
36
37
38 (36) Lide, D. R. *CRC Handbook of Chemistry and Physics, 85th Edition*; CRC Handbook of
39 Chemistry and Physics, 85th Ed; Taylor & Francis, 2004.
40
41
42
43
44
45
46
47
48
49
50
51
52
53
54
55
56
57
58
59
60

- 1
2
3 (37) Zhang, H.; Banfield, J. F. Energy Calculations Predict Nanoparticle Attachment
4
5 Orientations and Asymmetric Crystal Formation. *J. Phys. Chem. Lett.* **2012**, *3*, 2882–
6
7 2886.
8
9
10
11
12
13
14
15
16
17
18
19
20
21
22
23
24
25
26
27
28
29
30
31
32
33
34
35
36
37
38
39
40
41
42
43
44
45
46
47
48
49
50
51
52
53
54
55
56
57
58
59
60

TOC graphic

